# Detection of a defect on the back of a pipe by non-contact remote measurements

**Takahiro Hayashi**
Graduate School of Engineering, Kyoto University
Kyoto-daigaku Katsura Nishikyo-ku, Kyoto 615-8540, Japan
hayashi@kuaero.kyoto-u.ac.jp

## ABSTRACT

*Pipe inspection is generally executed with ultrasonic pulse echo testing where a small range of pipe wall under an ultrasonic transducer can be evaluated in one measurement. Costly and laborious point-by-point testing is required if a whole range of a pipe should be inspected. The author has investigated fast defect imaging for a plate-like structure using a scanning laser source (SLS) technique as an efficient defect inspection technique. Although the imaging technique is feasible in non-contact remote measurements, only a plate cross-section under the laser irradiation surface can be evaluated. This study describes detection of wall thinning on the back of a pipe using resonance of guided wave propagating in a pipe circumference by non-contact remote measurements with the SLS technique. The narrowband elastic waves are generated in a pipe by modulating laser pulses with fiber laser equipment. When the modulation frequency is in harmony with the resonance frequency of a circumferential guided wave, the distribution of the frequency spectrum peak obtained with the SLS technique become identical to the resonance pattern of the circumferentially guided wave mode. The distributions are distorted for a pipe with wall thinning on the back indicating that this technique has a potential for detection of defects on the back of a pipe.*

## 1 INTRODUCTION

Non-destructive evaluation (NDE) using elastic waves generated by laser irradiation to industrial material is widely known as laser ultrasonics [1-3]. In laser ultrasonics, a broadband ultrasonic wave in the frequency of MHz range generated by a laser pulse with a pulse width of the order of ns is generally used for inspecting and evaluating materials. Because a broadband pulse wave having superior characteristics in resolution of time and space is easily generated in industrial materials at a high peak power using commercially available laser equipment such as a Nd: YAG laser, it has become standard in laser ultrasonics.

However, a broadband pulse wave cannot be used under experimental conditions at low signal to noise ratio (SNR) because it is easily buried in noise. Also, increasing the maximum power of laser pulse for improving SNR causes damage on a surface of a material due to ablation. In order to improve SNR at low maximum power, the authors developed narrowband elastic wave generation using fiber laser equipment that has become popular in laser processing [4-6]. Fiber laser equipment can generate laser pulses at a high repetition rate on the order of a few hundred kHz or MHz. Modulating such high repetition laser pulses can output intermittent laser pulse trains, which results in generation of elastic waves corresponding to the modulation signal. The authors experimentally demonstrated in [6] that the use of long duration modulation signal significantly improves SNR in frequency domain, and this technique was applied to defect imaging by an SLS technique.

In the SLS technique, a laser generates an elastic wave, and the laser source is scanned over a material while the elastic wave is detected at a fixed position. This leads to stable measurements of multiple waveforms. Moreover, it was experimentally proved that the SLS technique is effective for surface crack detection. Kromine et al. [7] and Sohn et al. [8, 9] detected surface cracks with a high precision by Rayleigh wave measurements with SLS. Takatsubo et al. [10] created a movie of ultrasonic waves propagating on the surface of a material from waveforms obtained by the SLS technique and proved that defects can be detected from the wave distortions at the defects. Dixon et al. [11] observed ultrasonic wave enhancement when the laser source was located in the vicinity of a surface crack, and Clough et al. [12, 13] detected a surface crack with high precision using this phenomena.

The authors have investigated defect imaging using multiple waveforms measured by SLS [4-6], [14-17]. This defect imaging technique uses the phenomena that the generation energy of a flexural wave varies with plate thickness and defect depth near the laser source, and, therefore, this imaging technique can be applied to a complex plate structure in which there are no straight paths from a laser source to a receiver [4]. In reference [5], we developed a fast imaging system for a plate-like structure using a feature of SLS that allows multiple waveforms to be detected stably by a fixed receiver. In order to measure flexural vibration of a plate from a remote position, a laser Doppler vibrometer (LDV) is required as a receiving devise. Because an LDV reduces SNR significantly compared with such contact devices as ultrasonic transducers and piezo-electric transducers, the narrowband wave generation by a fiber laser was

adopted to improve SNR, and defect imaging from a remote position was realized [5, 18]. Since this imaging technique has prominent features of fast remote non-contact imaging, images of inner defects as well as surface defects of plate-like structures are obtained as with optical and infrared cameras.

Moreover, the authors proved that defect imaging with SLS, called Elastic wave camera (E-camera), can be applied to curved plates such as pipes. Defect images were experimentally obtained for straight and branched pipes [18]. However, this imaging technique using an E-camera can be applied only to plate regions on which a laser can be irradiated. In the case of pipework, half of the circular cross-section can be evaluated using an E-camera. Namely, the defect imaging with an E-camera system still has the issue that the other half region on the back of the pipe cannot be evaluated.

This study investigates detection of wall thinning on the back of a pipe using resonance of circumferential guided waves generated by laser. In the second chapter, guided waves propagating in the circumferential directions are discussed with dispersion curves and wave structures on a pipe cross-section. In chapter 3, the pipe specimen used and the experimental system, including fiber laser equipment and LDV, are described. Finally, experimental results are shown in chapter 4.

## 2 GUIDED WAVES PROPAGATION IN THE CIRCUMFERENTIAL DIRECTIONS

Defect imaging by SLS uses flexural vibration generated by laser irradiation onto a plate and a pipe [19]. The propagation mode in a plate with flexural vibration is only the fundamental anti-symmetric mode, called the A0 mode, in a small frequency-

thickness product range. Defect images were obtained by variations of generation energy of the A0 mode with a plate thickness and existence of defects in the vicinity of a laser source. In the case of a pipe, a large number of flexural vibration modes exist, and they all have different circumferential distributions as well as thickness distributions, and different phase and group velocities. Figures 1 (a) and (b) are phase velocity dispersion curves and group velocity dispersion curves of guided waves propagating in the longitudinal direction of an aluminum alloy pipe of 3.0 mm thick with a 100 mm outer diameter, whose dimensions are the same as pipes in the experiments shown later. These curves were calculated with a semi-analytical finite element (SAFE) method [20-22] using longitudinal and transverse velocities of 6260 m/s and 3000 m/s, respectively. In the SAFE method, displacement distributions on a pipe cross-section for guided wave modes are also calculated, as well as the dispersion curves. In Figs. 1 (a) and (b), flexural vibrations dominated by the displacement in the thickness direction are shown with solid lines. Guided wave modes generated by laser shots are the flexural vibrations shown with the solid lines. The circumferential order $n$ in Fig. 1 (a) indicates that the mode has a displacement distribution of $\exp(\pm in\theta)$. When a laser source is located at $\theta = 0$, flexural vibrations propagate in the $\pm\theta$ directions symmetrically, and the distribution of the harmonic flexural waves result in $\exp(+in\theta) + \exp(-in\theta)$ $= 2\cos(n\theta)$. Figure 2 shows the schematic figures of the circumferential displacement distributions from $n = 0$ to 11. If considering that dashed circles are the original position of a pipe surface, each mode with a different circumferential order vibrates between black solid lines and gray solid lines in the out-of-plane direction. For example, for $n$=0,

FIG.1

$\exp(+in\theta)+\exp(-in\theta)=2$, and, then, the displacement distribution does not depend on $\theta$ and becomes symmetric with respect to the pipe center, as shown in Fig. 2 (a). For $n$=1, $\exp(+in\theta)+\exp(-in\theta)=2\cos\theta$, and, then, the displacement distributes in the cosine function with one period in one round of the circle, as shown in Fig. 2 (b). This is described in detail in the author's previous papers [23, 24].

The cutoff frequencies shown by the arrows in Fig. 1 provide infinite values in phase velocities, zeros in group velocities, and infinite wavelengths in the longitudinal direction. This means that the harmonic waves at the cutoff frequencies have uniform distribution in the longitudinal direction and become standing waves in the circumferential direction, as shown in Fig. 2. In other words, the cutoff frequencies denote resonance frequencies of the circumferential guided waves. Nishino et al. developed a precise measurement technique of pipe thickness using the circumferential standing waves [25].

FIG.2

In the experiments shown later, wall thinning is detected using the characteristics that wall thinning disturbs the circumferential resonant modes at the cutoff frequencies.

**3 EXPERIMENTAL SET-UP AND PIPE SPECIMEN USED**

In the experiments described here, a fiber laser and an LDV were used for generating and detecting elastic waves, as shown in Fig. 3. The fiber laser equipment used in this experiment can generate laser pulses at a high repetition rate, and the laser output can be controlled by external modulation signals. In our previous studies [4-6],

FIG.3

the use of the fiber laser and external modulation signals enabled us to generate long-duration burst waves in plate-like structures. Because the use of a burst wave improves SNR in the frequency domain, defect images were successfully obtained using such a low sensitive receiving device as an LDV [6, 18]. The same system was used in this study. The repetition frequency of the fiber laser was 580 kHz, and the external modulation signals were rectangular burst waves with a duration time of 2 ms at frequencies of 5 kHz to 40 kHz. Waveforms were recorded with an analog-digital converter for 20 ms after the moment of laser shot, and then the peak values of their Fourier spectra were obtained using a personal computer.

Aluminum alloy pipes with an outer diameter of 100 mm, pipe wall thickness of 3.0 mm, and length of 500 mm were used as pipe specimens. An intact pipe with uniform thickness was used in section 4.1, and a pipe specimen with artificial wall thinning inside the pipe was used in section 4.2. The artificial defect as shown in Fig. 4 was made with a lathe, in which the tip of a tool rotated in a diameter of 65 mm, and the rotation center gradually moved away from the pipe center to adjust the minimum thickness of the wall thinning to 1.5 mm. The distance between the test pipe and the experimental system was about 3.0 m in these laboratory tests. Although the distance must be longer like 10 m or 20 m in a practical use, there seems to be no crucial problems to execute such remote measurements, because the LDV supports such distances and elastic waves can be generated when a laser spot is appropriately focused on the pipe surface.

FIG.4

## 4 EXPERIMENTAL RESULTS

### 4.1 Resonance patterns in an intact pipe

Guided waves in an intact pipe with uniform thickness were measured using the non-contact experimental system. As shown in Figs. 5 (a) and (b), the receiving point was located at the right edge center of the pipe, and the circumferential position of this point was set to $\theta = 0°$. The laser source point was located 20 mm away from the receiving point. The pipe was supported with aluminum blocks at two points at the bottom of the pipe, $\theta = 270°$, as shown in Fig. 5. Two arrangements of the pipe supports were used in the experiments; one is the left edge with a longitudinal position 200 mm away from the right edge, as shown in Fig. 5 (a), and the other one is the left edge and the right edge, as shown in Fig. 5 (b).

FIG.5

For the pipe support arrangement shown in Fig. 5 (a), waveforms and their Fourier spectra are shown in Figs. 6 (a) and (b), respectively, for the modulation signals with durations of 2 ms and frequencies of 10.0 kHz and 14.3 kHz. Elastic waves generated by laser shots cannot be recognized in the signals at 10.0 kHz, Fig. 6 (a) gray, due to the large noise. However, a distinct frequency spectrum peak can be observed at 10 kHz in Fig. 6 (b) gray. In the frequency spectrum of Fig. 6 (b), a large peak appearing around 21 kHz is intrinsic noise generated in the LDV, and the noise is largely contained in the waveforms of Fig. 6 (a). At 14.3 kHz, the waveform exceeding the noise is obtained as shown in Fig. 6 (a) black. The waveform maintains a high amplitude over the whole time range of 20 ms even though the laser output stopped at 2 ms. This implies that resonance in the pipe was detected at 14.3 kHz.

FIG.6

FIG.7

Figure 7 (a) is variation of the frequency spectrum peak with the modulation frequency. In the pipe support arrangement of Fig. 5 (a), the values of the frequency spectrum peaks in the frequency range of the modulation frequency±0.25 kHz were plotted when the frequency of the modulation signal was changed from 5 kHz to 40 kHz with 0.1 kHz increments. A large peak was obtained at 14.3 kHz, which indicates that the waveform and its frequency spectra, shown with black lines in Fig. 6 (a) and (b), are under the resonance condition. From Fig. 7 (a), the resonance frequencies are 7.2 kHz, 10.5 kHz, 18.6 kHz, 23.4 kHz, 28.7 kHz, and 34.4 kHz, and the peak around 21 kHz is the effect of intrinsic noise, as seen in Fig. 6 (b). These frequencies correspond to the cutoff frequencies of $n$=5 to 11. Namely, these resonances are caused by the standing waves in the circumferential direction.

The frequency spectrum peak value was plotted in Fig. 7 (b) when a pipe support was located at the same longitudinal position as the generation and receiving points shown in Fig. 5 (b). The resonance modes of the even order of $n$=6, 8, and 10 are significantly reduced, while the resonance modes of the odd order of $n$ =5, 7, 9, and 11 are still large. These results indicate the difference of resonant modes with the antinode and node at the circumferential position of the pipe support $\theta = 270°$. The even order modes shown in Figs. 2 (a), (c), (e), (g), (i), and (k) have an antinode at $\theta = 270°$, while the odd order modes shown in Figs. 2 (b), (d), (f), (h), (j), and (l) have a node at $\theta = 270°$. In Fig. 7 (b), the modes with an antinode at the pipe support did not resonate due to the energy leakage into the pipe support. However, the modes with a node at the pipe support resonated without influence of the pipe support.

Next, distributions of the frequency spectrum peak were obtained in Fig. 8 when a laser source was scanned over the whole pipe at the resonance frequencies. The pipe supports and the receiving point were located at the same positions depicted in Fig. 5 (b). The laser source was scanned over a range of 520 mm × 110 mm at 2 mm increments, and the peak values of the frequency spectra obtained at all of the rastering positions were plotted in gray scale. A small gray square appearing at the right edge of the region is due to the retro-reflection tape for LDV detection. The values at the point 20 mm apart from the tape correspond to the values at the frequencies in Fig. 7 (b). A horizontal striped pattern stretching over the entire pipe is clearly observed in Fig. 8 (a). This pattern, consisting of five antinodes and four nodes, indicates the resonance mode of $n$=5, which agrees well with the mode in Fig. 2 (f). Although a horizontal strip pattern can also be seen in Fig. 8 (b), the intensity is small in the whole region due to the energy leakage into the pipe support, as seen in Fig. 7 (b). In Fig. 8 (c), the right half region consists of 7 antinodes and 6 nodes, which indicates the resonance mode of $n$=7. Fig. 8 (g) also shows the resonance pattern for the corresponding circumferential order. In Fig. 8 (d)-(f), the horizontal strip patterns were not clear because other resonances also occur at those frequencies.

Now, we focus on the horizontal strip patterns for detection of defects on the back of a pipe using the SLS. Although the horizontal patterns were seen in Fig. 8 (c) and (g), the intensities become smaller at the further ranges from the receiving point. These results show that the resonance modes of $n$=7 and 11 become gradually smaller at remote distances between the laser source and receiver. As shown in Fig. 9, the elastic

FIG.9

wave generated by a laser shot propagates in all directions. Among them, only circumferentially propagating waves resonate at the cutoff frequencies. These modes do not propagate in the longitudinal direction at the cutoff frequencies. However, considering the modes at slightly higher frequencies, these modes can propagate with a very small group velocity and maintain resonance in the circumferential direction. These modes are spirally propagating modes in both circumferential directions. When a laser source and a receiving point are not close, the received waveforms are the spirally propagating modes. When they resonate in the cross-section of a pipe, the horizontal strip patterns are observed. Because the stripe bands become larger for smaller circumferential orders, *n*, the spirally propagating modes maintain resonance in spite of the inclination of the wave plane. On the other hand, for higher circumferential orders, even a small inclination in the spirally propagating modes suppresses the resonance. Comparing the experimental results of Figs. 8 (a), (c), and (g), the horizontal patterns are localized more at the receiving point for higher order modes due to the features of circumferential modes.

Hereafter, detection of artificial wall thinning is discussed for the circumferential orders *n*=5 (7.2 kHz) and *n*=7 (14.3 kHz), in which the horizontal strip patterns were largely obtained in Figs. 8 (a) and (c).

**4.2 Resonance patterns in a pipe with a defect on the back**

The horizontal resonance patterns generated by guided wave modes propagating in the circumferential directions were discussed above. It can be predicted

that the circumferential resonance patterns are changed due to obstacles such as defects and pipe supports. Therefore, in this section, distributions of frequency spectrum peak are discussed for a pipe with wall thinning on the back.

Figure 10 shows distributions of the frequency spectrum peak for the modulation signal of 7.2 kHz. The experimental settings are the same as written in section 4.1. The artificial wall thinning was located at the opposite side of the generation laser emission region, as shown in the schematic figure of Fig. 10 (d); if the receiving position is $\theta = 0°$, then the center of the wall thinning is $\theta = 180°$. Figures 10 (a) and (b) are distributions for left and right receiving positions, respectively. The dark areas at the left edge of the pipe are the regions affected by oily deposits adhered during machining. In both Figs. 10 (a) and (b), the horizontal striped patterns can be seen between the defect area and receiving point, because the resonance occurred appropriately at the frequency in this range. However, the resonance patterns are distorted and vertical patterns also appear in the vicinity of the defect area and further because the resonance cannot be measured clearly at the receiving point. Compared with the result for the intact pipe shown in Fig. 8 (a), these differences in the images are the effect of the wall thinning on the back. As the defect area cannot be located in Figs. 10 (a) and (b), respectively, the average of (a) and (b) are given in Fig. 10 (c). The vertical patterns are distributed symmetrically with respect to the defect area, which indicates that this image approximately shows the defect position.

Figures 11 (a) - (c) depict the distributions of the frequency spectrum peak at 14.3 kHz for the defect position at $\theta = 180°$, as shown in Fig. 11 (d). Like in Fig. 10, Figs.

FIG.11

11 (a) and (b) are from the left and right receiving positions, and Fig. 11 (c) shows the average of them. The horizontal patterns are disconnected at the defect area in (a) and (b), and, therefore, a small intensity region can be seen at the defect area in (c).

Figures 12 (a) and (b) are the averaged distributions at 7.2 kHz and 14.3 kHz, respectively, when the defect is located at $\theta = 235$. These figures were obtained using the same procedures used to obtain Fig. 10 (c) and Fig. 11 (c); only the circumferential locations of the wall thinning were different. These figures show similar tendencies as Fig. 10 (c) and Fig. 11 (c); the vertical patterns are symmetrically distributed from the defect area at 7.2 kHz, and a small intensity region appears at the defect area at 14.3 kHz.

FIG.12

As shown above, resonance patterns were distorted due to the presence of wall thinning. This proves that the distortions of the image in the resonance patterns enable the detection of defects on the back of a pipe using the SLS. Considering the experimental results where the circumferential locations of wall thinning did not change the distortions of the resonance patterns, it can be concluded that the circumferential position cannot be located using the processing techniques described here. However, resonance patterns may be affected by the circumferential position of defects considering the results in section 4.2, where the locations of a pipe support and nodes and antinodes of a circumferential mode affect the resonant amplitude. Using the circumferential modes appropriately, a circumferential position of defects may be predicted with further study.

## 5. Conclusions

This study discussed detection of a defect on the back of a pipe using resonances in the pipe circumference with the SLS measurement. First, it was confirmed that narrowband burst waves generated by modulated high-repetition laser pulses induced resonance in the pipe circumference at the cutoff frequencies of the guided waves in the pipe. In the frequencies, distributions of the frequency spectrum peak obtained by the SLS corresponded to the resonance patterns of the circumferential guided waves. The resonance patterns were distorted at the area where a defect was located on the back of the pipe, which is useful for defect detection in a pipe.

**ACKNOWLEDGMENT**

I would like to thank all the workshop staff at Kyoto University for their effort in the production of pipe specimens. This work was supported by JSPS KAKENHI, Grant Number 26282094, 17H02052, 18K18920, and Chubu Electric Power Co., Inc.

**REFERENCES**

[1] Scruby, C. B. and Drain, 1990, L. E., *Laser Ultrasonics: Techniques and Applications* , CRC press, ISBN: 9780750300506

[2] Mckie, A. D. W., and Addison, R. C., 1992, "Inspection of Components Having Complex Geometries Using Laser-Based Ultrasound," *Review of Progress in Quantitative Nondestructive Evaluation Volume*, pp. 577–584.

[3] Blouin, A., Levesque, D., Neron, C., Drolet, D., and Monchalin, J. P., 1998, "Improved Resolution and Signal-to-Noise Ratio in Laser-Ultrasonics by SAFT Processing.," Opt. Express, **2**(13), pp. 531–539.

[4] Hayashi, T., 2016, "Imaging Defects in a Plate with Complex Geometries," Appl. Phys. Lett., **108**(8), p. 81901.

[5] Hayashi, T., 2017, "High-Speed Non-Contact Defect Imaging for a Plate-like Structure," NDT E Int., **85**, pp. 53–62.

[6] Hayashi, T., and Ishihara, K., 2017, "Generation of Narrowband Elastic Waves with a Fiber Laser and Its Application to the Imaging of Defects in a Plate," Ultrasonics, **77** , pp. 47–53.

[7] Kromine, A. K., Fomitchov, P. A., Krishnaswamy, S., and Achenbach, J. D., 2000, "Laser Ultrasonic Detection of Surface Breaking Discontinuities: Scanning Laser Source Technique," Mater. Eval., **58**, pp. 173–177.

[8] Sohn, Y. H., and Krishnaswamy, S., 2004, "Interaction of a Scanning Laser-Generated Ultrasonic Line Source with a Surface-Breaking Flaw," J. Acoust. Soc. Am., **115**(1), pp. 172–181.

[9] Sohn, Y., and Krishnaswamy, S., 2006, "A near-Field Scanning Laser Source Technique and a Microcantilever Ultrasound Receiver for Detection of Surface-Breaking Defects," Meas. Sci. Technol., **17**(4), pp. 809–818.

[10] Takatsubo, J., Wang, B., Tsuda, H., and Toyama, N., 2007, "Generation Laser Scanning Method for the Visualization of Ultrasounds Propagating on a 3-D Object with an Arbitrary Shape," J. Solid Mech. Mater. Eng., **1**(12), pp. 1405–1411.

[11] Dixon, S., Cann, B., Carroll, D. L., Fan, Y., and Edwards, R. S., 2008, "Non-Linear Enhancement of Laser Generated Ultrasonic Rayleigh Waves by Cracks," Nondestruct. Test. Eval., **23**(1), pp. 25–34.

[12] Clough, A. R., and Edwards, R. S., 2014, “Scanning Laser Source Lamb Wave Enhancements for Defect Characterisation,” NDT E Int., **62**, pp. 99–105.

[13] Clough, A. R., and Edwards, R. S., 2015, “Characterisation of Hidden Defects Using the near-Field Ultrasonic Enhancement of Lamb Waves,” Ultrasonics, **59**, pp. 64–71.

[14] Hayashi, T., Murase, M., and Salim, M. N., 2009, “Rapid Thickness Measurements Using Guided Waves from a Scanning Laser Source.,” J. Acoust. Soc. Am., **126**(3), pp. 1101–1106.

[15] Hayashi, T., Murase, M., and Kitayama, T., 2012, “Frequency Dependence of Images in Scanning Laser Source Technique for a Plate.,” Ultrasonics, **52**(5), pp. 636–42.

[16] Salim, M. N., Hayashi, T., Murase, M., Ito, T., and Kamiya, S., 2012, “Fast Remaining Thickness Measurement Using a Laser Source Scanning Technique,” Mater. Trans., **53**(4), pp. 1–7.

[17] Hayashi, T., Murase, M., Ogura, N., and Kitayama, T., 2014, “Imaging Defects in a Plate with Full Non-Contact Scanning Laser Source Technique,” Mater. Trans., **55**(7), pp. 1045–1050.

[18] Hayashi, T., and Fukuyama, M., 2016, “Vibration Energy Analysis of a Plate for Defect Imaging with a Scanning Laser Source Technique,” J. Acoust. Soc. Am., **140**(4), pp. 2427–2436.

[19] Hayashi T., Under review, “Non-contact imaging of pipe thinning using elastic guided waves generated and detected by lasers,” International Journal of Pressure Vessels and Piping.

[20] Hayashi, T., Kawashima, K., Sun, Z., and Rose, J. L., 2003, “Analysis of Flexural Mode Focusing by a Semianalytical Finite Element Method.,” J. Acoust. Soc. Am., **113**(3), pp. 1241–1248.

[21] Hayashi, T., Song, W.-J., and Rose, J. L., 2003, “Guided Wave Dispersion Curves for a Bar with an Arbitrary Cross-Section, a Rod and Rail Example,” Ultrasonics, **41**(3), pp. 175–183.

[22] Hayashi, T., Tamayama, C., and Murase, M., 2006, “Wave Structure Analysis of Guided Waves in a Bar with an Arbitrary Cross-Section.,” Ultrasonics, **44**(1), pp. 17–24.

[23] Hayashi, T., and Murase, M., 2005, “Mode Extraction Technique for Guided Waves in a Pipe,” Nondestruct. Test. Eval., **20**(1), pp. 63–75.

[24] Hayashi, T., Nagao, M., and Murase, M., 2008, “Defect Imaging with Guided Waves in a Long Pipe,” J. Solid Mech. Mater. Eng., **2**(7), pp. 888–899.

[25] Nishino, H., Asano, T., Taniguchi, Y., Yoshida, K., Ogawa, H., Takahashi, M., and Ogura, Y., 2011, “Precise Measurement of Pipe Wall Thickness in Noncontact Manner Using a Circumferential Lamb Wave Generated and Detected by a Pair of Air-Coupled Transducers,” Jpn. J. Appl. Phys., **50**, 07HC10-1 - 07HC10-7

## Figure Captions List

Fig. 1 Dispersion curves for an aluminum alloy pipe

Fig. 2 Circumferential variations for different circumferential mode orders

Fig. 3 Experimental set-up

Fig. 4 Pipe specimen with artificial wall thinning

Fig. 5 Pipe support arrangements and generation and receiving points

Fig. 6 Waveforms and their frequency spectra for the pipe support arrangement shown in Fig. 5 (a)

Fig. 7 Frequency spectrum peak variations with frequency.

Fig. 8 Distributions of frequency spectrum peak for an intact pipe. The arrangement of the pipe supports and the receiving position is as shown in Fig. 5 (b).

Fig. 9 Schematic figure of spirally propagating waves

Fig. 10 Distributions of frequency spectrum peak at 7.2 kHz

Fig. 11 Distributions of frequency spectrum peak at 14.3 kHz

Fig. 12 Sum of distributions of frequency spectrum peak for left and right receiving positions when wall thinning is located at $\theta$=235°

Fig. 1 Dispersion curves for an aluminum alloy pipe.

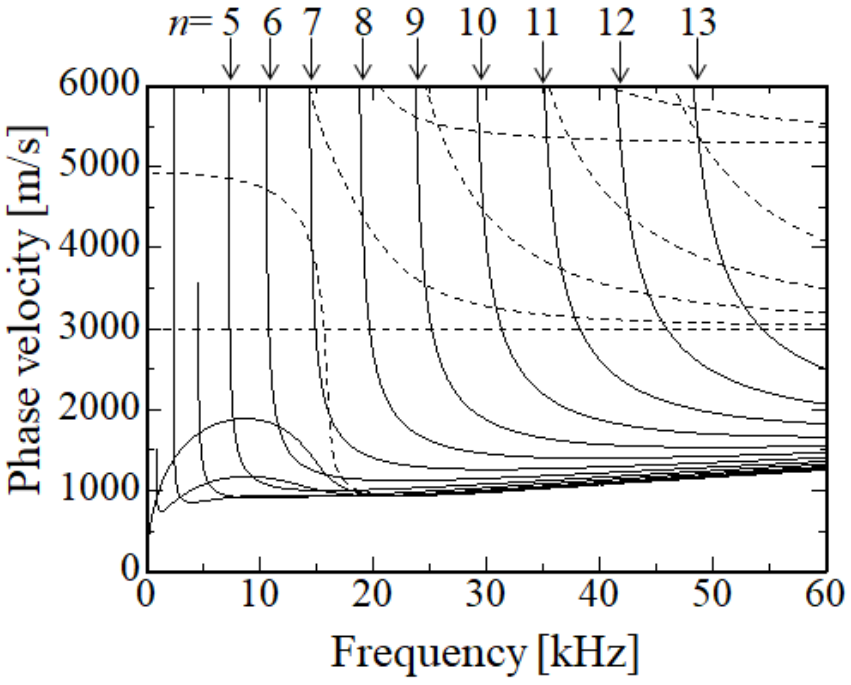


(a) Phase velocity

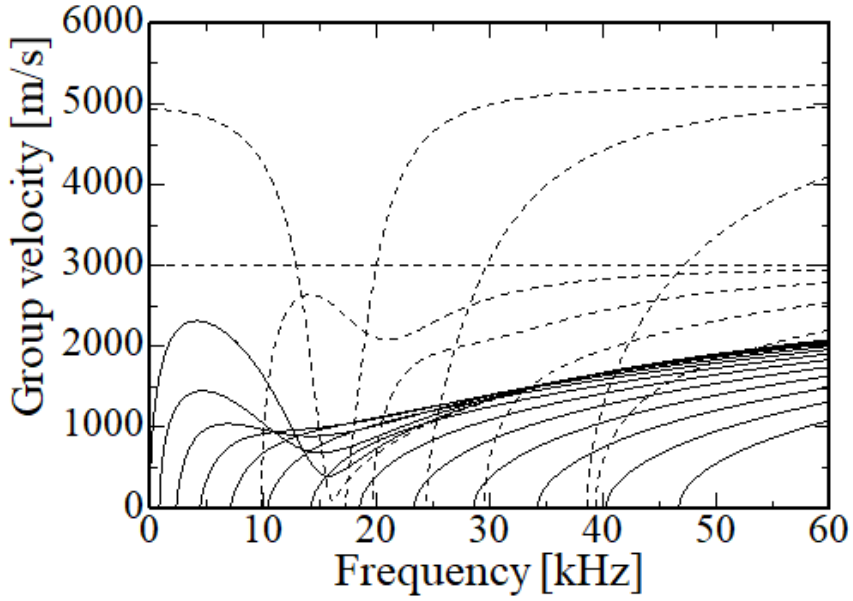


(b) Group velocity

Fig. 2. Circumferential variations for different circumferential mode orders.

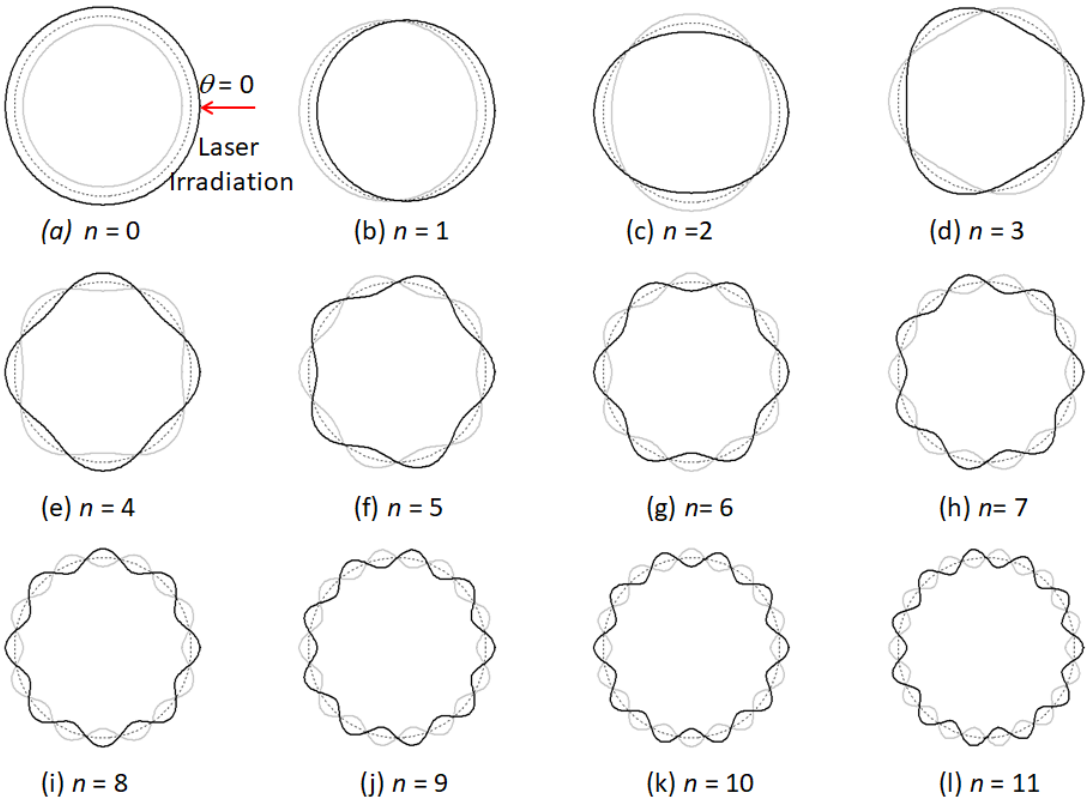

Fig. 3. Experimental set-up

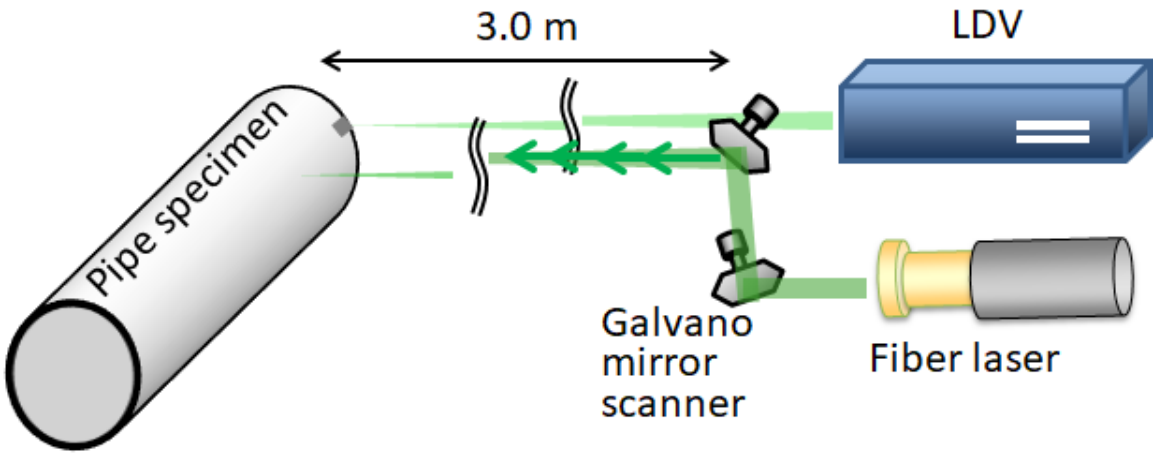

Fig. 4. Pipe specimen with artificial wall thinning.

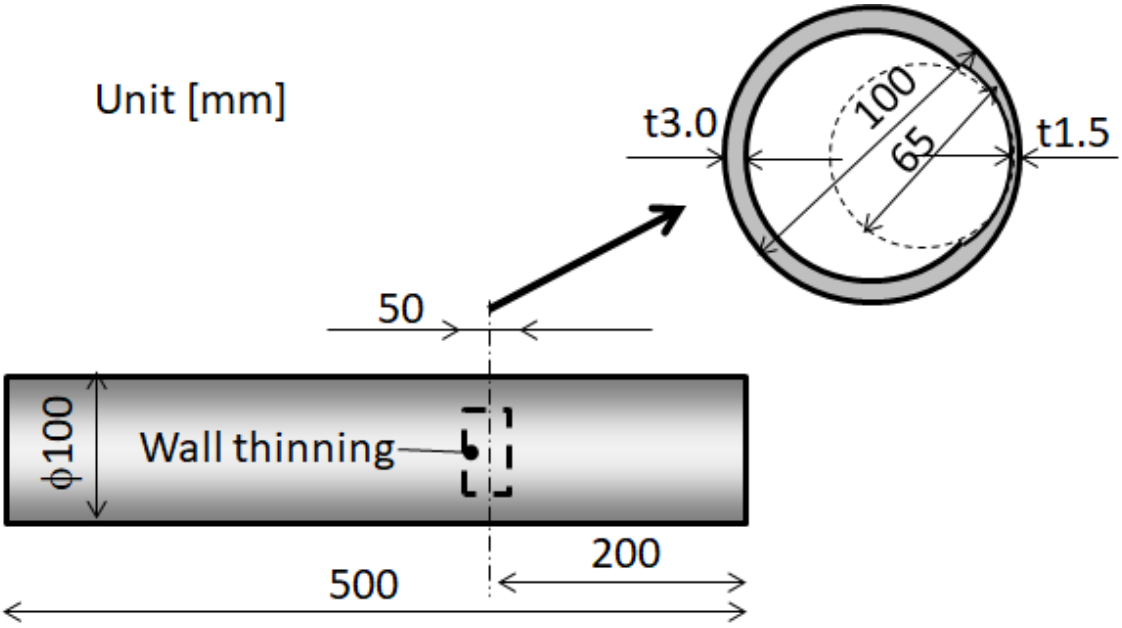

Fig. 5. Pipe support arrangements and generation and receiving points.

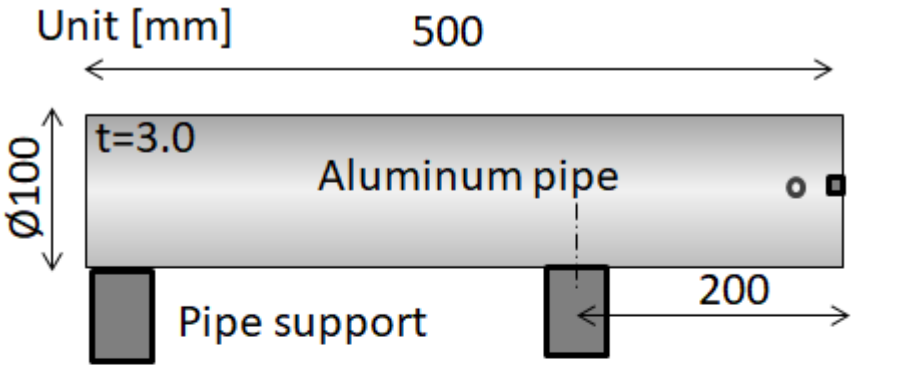


(a) Experiments shown in Figs. 6 and 7 (a)

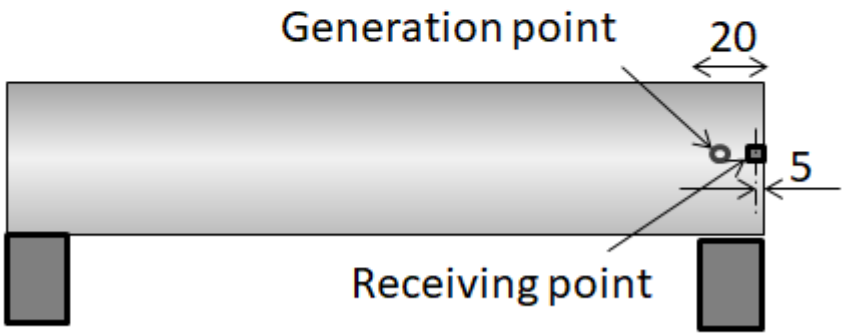


(b) Experiments shown in Fig. 7(b)

Fig. 6. Waveforms and their frequency spectra for the pipe support arrangement shown in Fig. 5 (a).

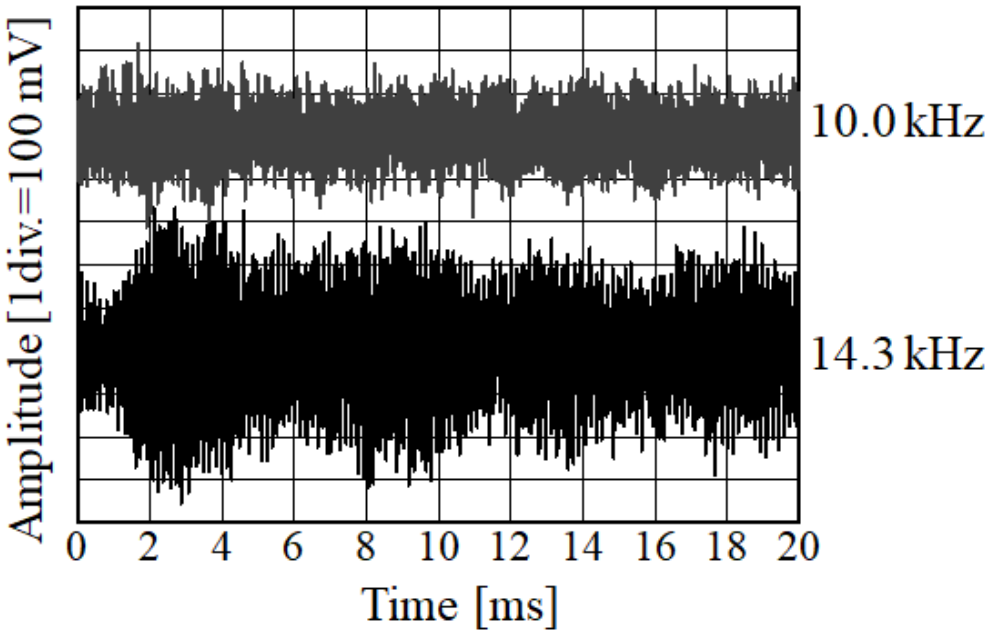


(a) Waveforms

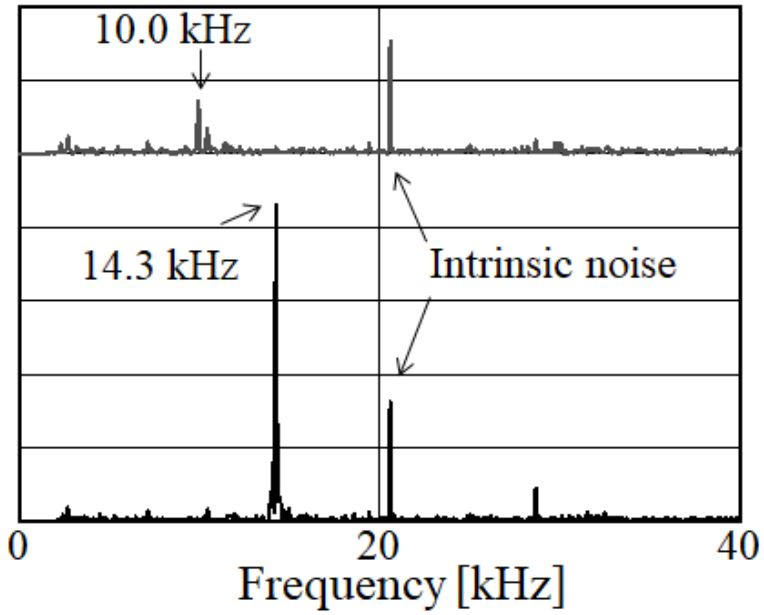


(b) Fourier spectra

Fig. 7. Frequency spectrum peak variations with frequency.

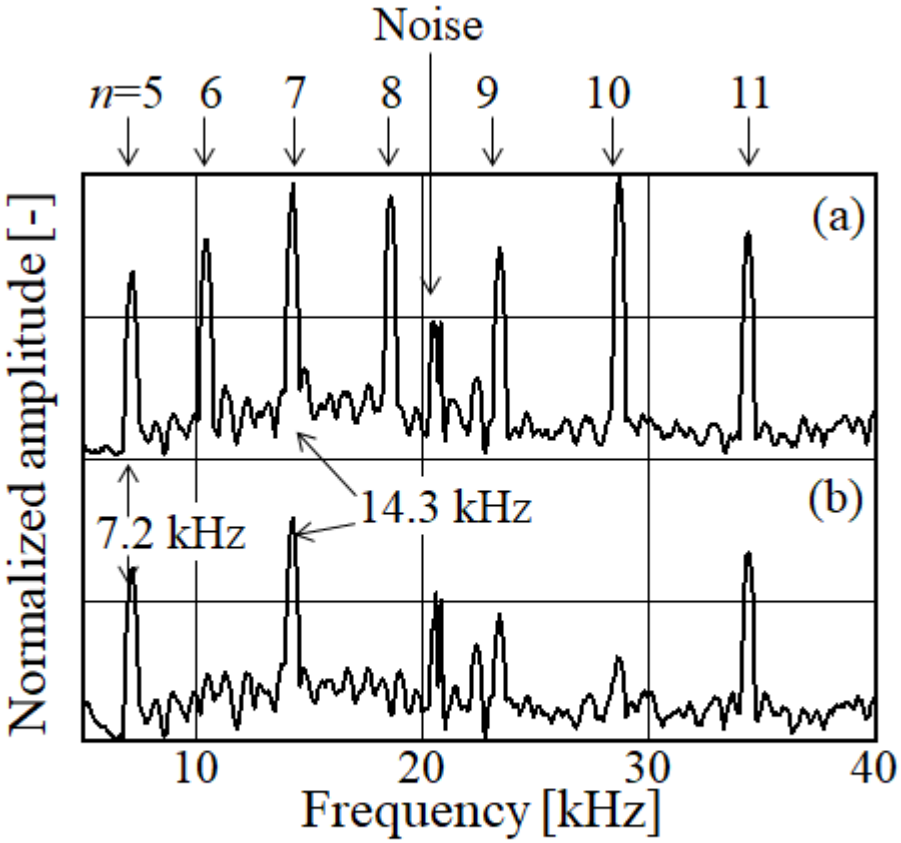


(a) Pipe support arrangement of Fig. 5 (a)
(b) Pipe support arrangement of Fig. 5 (b)

Fig. 8. Distributions of frequency spectrum peak for an intact pipe. The arrangement of the pipe supports and the receiving position is as shown in Fig. 5 (b).

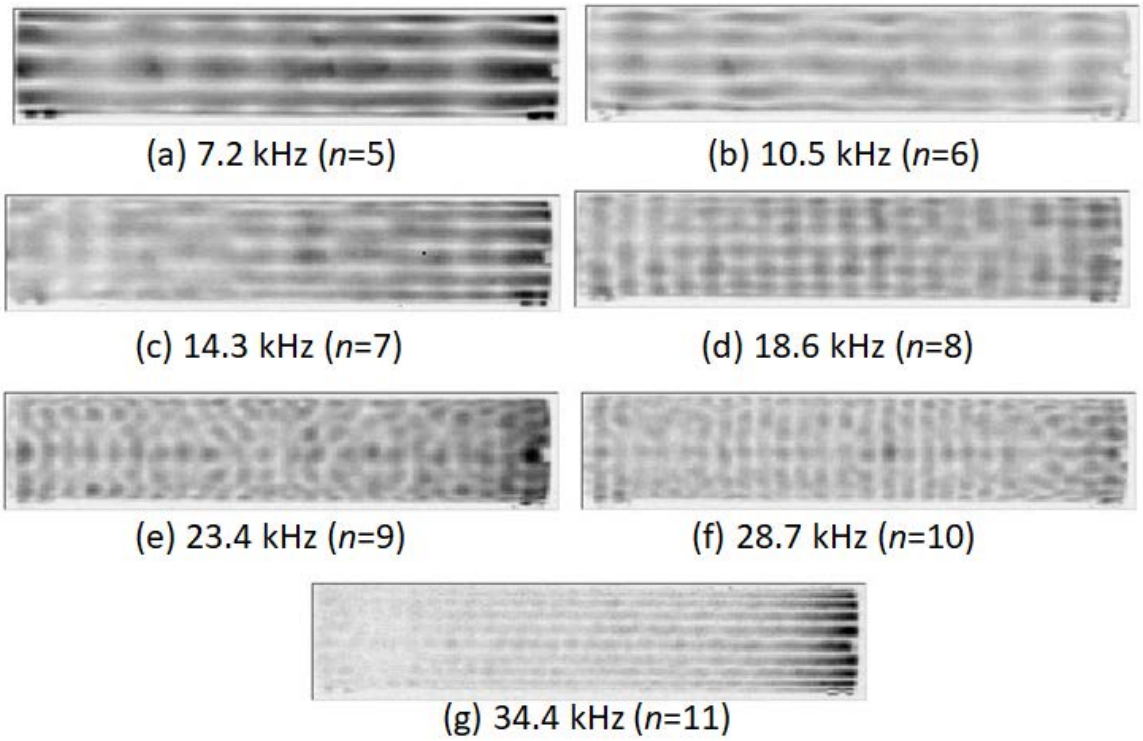

Fig. 9. Schematic figure of spirally propagating waves

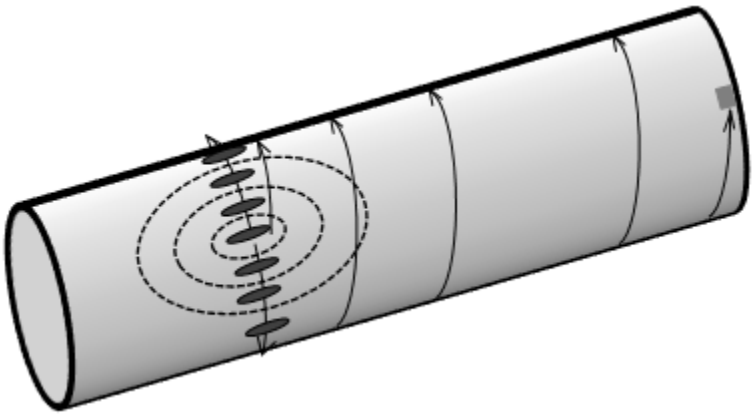

Fig. 10. Distributions of frequency spectrum peak at 7.2 kHz

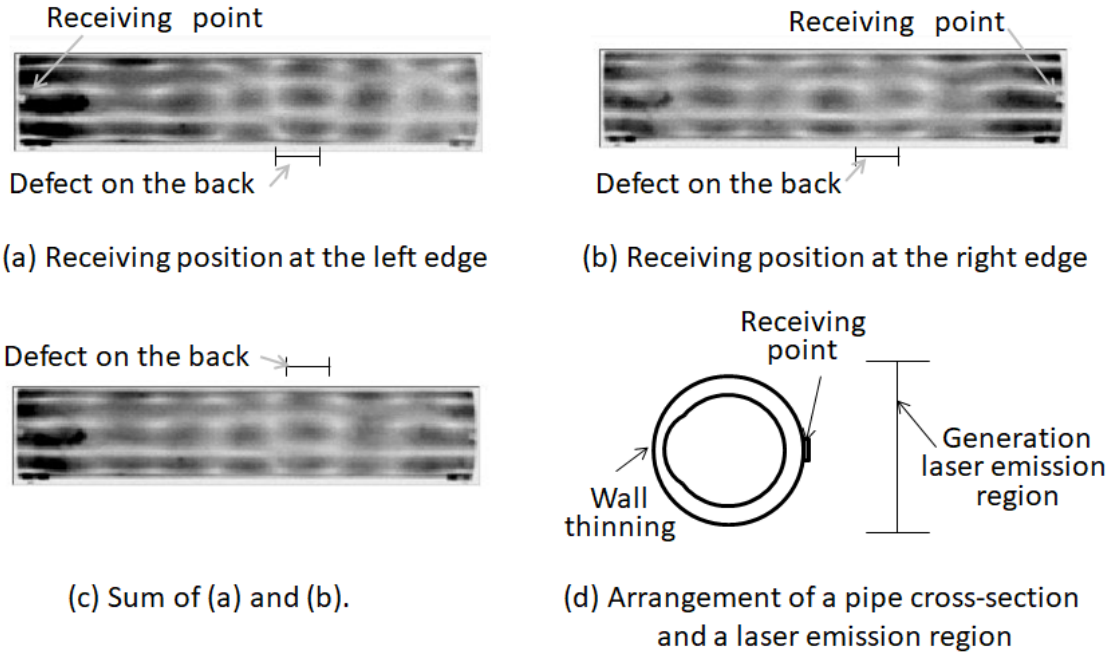

Fig. 11. Distributions of frequency spectrum peak at 14.3 kHz

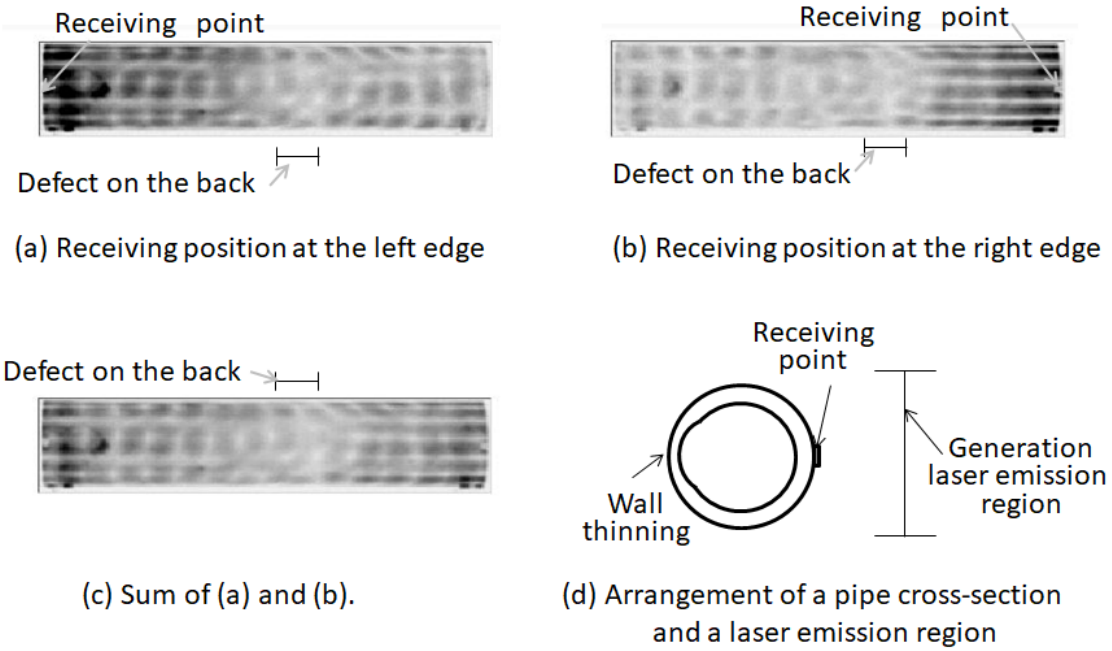

Fig. 12. Sum of distributions of frequency spectrum peak for left and right receiving positions when wall thinning is located at θ=235°.